symmetry

MDPI

Article

Multistep Model Predictive Control for Electrical Drives—A Fast Quadratic Programming Solution

Haotian Xie [1], Jianming Du [2], Dongliang Ke [3], Yingjie He [1], Fengxiang Wang [3,*], Christoph Hackl [2], José Rodríguez [4] and Ralph Kennel [1]

1 Electrical Drive Systems and Power Electronics, Technical University of Munich, 80333 München, Germany; haotian.xie@tum.de (H.X.); yingjie.he@tum.de (Y.H.); ralph.kennel@tum.de (R.K.)
2 Laboratory of Renewable Energy Systems, University of Applied Sciences Munich, 80335 München, Germany; jianming.du@hotmail.com (J.D.); christoph.hackl@hm.edu (C.H.)
3 National Local Joint Engineering Research Center for Electrical Drives and Power Electronics, Quanzhou Institute of Equipment Manufacturing, Haixi Institute, Chinese Academy of Sciences, Jinjiang 362200, China; dongliang.ke@fjirsm.ac.cn
4 Department of Engineering Sciences, Universidad Andres Bello, Santiago 7500971, Chile; jose.rodriguez@unab.cl
* Correspondence: fengxiang.wang@fjirsm.ac.cn; Tel.: +595-68181288

Abstract: Due to its merits of fast dynamic response, flexible inclusion of constraints and the ability to handle multiple control targets, model predictive control has been widely applied in the symmetry topologies, e.g., electrical drive systems. Predictive current control is penalized by the high current ripples at steady state because only one switching state is employed in every sampling period. Although the current quality can be improved at a low switching frequency by the extension of the prediction horizon, the number of searched switching states will grow exponentially. To tackle the aforementioned issue, a fast quadratic programming solver is proposed for multistep predictive current control in this article. First, the predictive current control is described as a quadratic programming problem, in which the objective function is rearranged based on the current derivatives. To avoid the exhaustive search, two vectors close to the reference derivative are preselected in every prediction horizon. Therefore, the number of searched switching states is significantly reduced. Experimental results validate that the predictive current control with a prediction horizon of 5 can achieve an excellent control performance at both steady state and transient state while the computational time is low.

Keywords: predictive current control; quadratic programming; multistep; fast solver; symmetry topology

Citation: Xie, H.; Du, J.; Ke, D.; He, Y.; Wang, F.; Hackl, C.; Rodríguez, J.; Kennel, R. Multistep Model Predictive Control for Electrical Drives—A Fast Quadratic Programming Solution. *Symmetry* **2022**, *14*, 626. https://doi.org/10.3390/sym14030626

Academic Editor: Christos Volos

Received: 2 March 2022
Accepted: 14 March 2022
Published: 21 March 2022

1. Introduction

Model predictive control (MPC) was initially employed in the process industry with slow dynamic in the 1970s [1–3]. The main concept centers around solving an optimization problem online by predicting the future behavior of the control plant [4,5]. With the tremendous development of digital processors, the computational capability of the controllers has been significantly increased in the recent decade, which enables MPC to be applied in power electronics applications, e.g., railway transportation and wind turbines [6,7]. Due to its merits of simple concept, flexible inclusion of constraints and the ability to handle optimization problems with multiple control targets, MPC has become an alternative control strategy for power converters [8,9].

Categorized by the type of control inputs, MPC can be divided into two mainstream categories, continuous control set MPC (CCS-MPC) and finite control set MPC (FCS-MPC) [10]. In CCS-MPC, the reference voltage vector is obtained by tracking the predicted control variable along with its reference value [11]. The optimal vectors and their duty cycles are calculated in the modulation stage. On the contrary, FCS-MPC directly searches

all the voltage vectors to evaluate the tracking error between the predicted value and the reference value. The optimal vector is selected by minimizing the tracking error in the formulated cost function [12]. Considering the discrete nature of the switching sequences, FCS-MPC becomes one of the predominant control strategies for the power converters. Compared with direct torque control (DTC), FCS-MPC overcomes the drawback of high torque ripples at steady state. Moreover, FCS-MPC achieves the merit of fast dynamic response when compared with field-oriented control (FOC) [13].

Regarding the diversity of control targets, FCS-MPC is classified by predictive current control (PCC), predictive torque control (PTC) and predictive speed control (PSC) and so on [14]. To obtain better current quality for the electrical drive systems, the stator current is selected as the control target in PCC. However, only one single voltage vector is applied in each sampling period of the PCC strategy. Therefore, PCC is still penalized by the large steady-state ripples because the reference vector can not be exactly tracked by the discrete voltage vector [15]. Although the steady-state errors can be reduced by employing multiple vectors, the number of applied vectors in each sampling period is increased, which results in higher switching frequency [16].

To improve the current quality while retaining low switching frequency, the PCC strategy can be implemented with a longer prediction horizon. However, the number of searched control inputs grows exponentially with the increased number of prediction horizons. In [17], a multistep FCS-MPC algorithm for a three-level inverter is proposed. The proposed algorithm achieves lower current distortion for a longer prediction horizon and low switching frequency. However, the issue of high computational burden has not been fully investigated. In [18], a computationally efficient FCS-MPC for the wind turbine system is proposed, in which the hexagon and triangle candidate regions are applied to reduce the algorithm complexity. However, the proposed algorithm is conducted with a short prediction horizon of 1. The high computational burden as a result of a longer horizon has not been addressed. In [19], a multistep MPC strategy is proposed for the H-bridge converter. The optimization problem is converted to an integer least-squares (ILS) problem, to be solved by a fast sphere decoding algorithm (SDA). However, the control variables in the proposed strategy are projected on the voltage vector, in which the additional constraint is included by the finite set. Moreover, the common-mode voltage is penalized in the objective function of the proposed method. In [20], a long-horizon FCS-MPC with non-recursive SDA is implemented on an FPGA. The effectiveness of the proposed method with a horizon of 5 steps is experimentally validated. Although the previous literature has proposed several solutions to reduce the computational burden of multistep FCS-MPC strategies, how to effectively reduce the algorithm complexity is still an open issue for further investigation.

To tackle the aforementioned issue, a fast quadratic programming (QP) solution for the multistep MPC strategy of electrical drive systems is proposed in this paper. First, the PCC optimization problem is regarded as a quadratic programming problem via a geometric perspective. Based on the above, the objective function is reformulated as the quadratic Euclidean norm of the predicted and reference current derivative. Instead of an exhaustive search, two current derivative vectors close to the reference are selected for optimization. Finally, the proposed algorithm is experimentally verified on the 2.2 kW induction machine testbench. It is validated that the proposed algorithm with a prediction horizon of 5 can significantly reduce the computational burden and achieve an excellent steady-state and transient-state performance.

The rest of this article is organized as follows. In Section 2, the description of the control plant is presented. The principle of multistep PCC algorithm is proposed in Section 3. In Section 4, a fast QP solution for multistep PCC algorithm is proposed. The proposed algorithm is experimentally validated and compared with the conventional PCC method in Section 5. Section 6 presents the conclusion and discussion of future work.

2. Control Plant Description

In this work, the squirrel-cage induction machine (IM) and the two-level voltage source inverter (2-L VSI) are considered as the control plant. The mathematical model of IM in the stationary frame is expressed in (1) to (4) [14].

$$u_{s\alpha,\beta} = R_s \cdot i_{s\alpha,\beta} + \frac{\mathrm{d}\psi_{s\alpha,\beta}}{\mathrm{dt}} \tag{1}$$

$$0 = R_r \cdot i_{r\alpha,\beta} + \frac{\mathrm{d}\psi_{r\alpha,\beta}}{\mathrm{dt}} - j\omega \cdot \hat{\psi}_{r\alpha,\beta} \tag{2}$$

$$\psi_{s\alpha,\beta} = L_s \cdot i_{s\alpha,\beta} + L_m \cdot i_{r\alpha,\beta} \tag{3}$$

$$\psi_{r\alpha,\beta} = L_m \cdot i_{s\alpha,\beta} + L_r \cdot i_{r\alpha,\beta} \tag{4}$$

where $u_{s\alpha,\beta}$ denotes the applied voltage vector for the 2-L VSI, $i_{s\alpha,\beta}$ and $i_{r\alpha,\beta}$ are the stator and rotor current, $\psi_{s\alpha,\beta}$ and $\psi_{r\alpha,\beta}$ are the stator and rotor flux, R_s and R_r are the stator and rotor resistances, L_s and L_r are the stator and rotor inductances, L_m is the magnetizing inductance and ω represents the angular rotor speed.

The topology of 2-L VSI and its applied voltage vectors are shown in Figure 1. u_0–u_7 are the applied switching events. $S_i = 0$ denotes that the upper power device turns off, $S_i = 1$ means that the upper power device turns on and $i = a,b,c$. The applied voltage vector u_s can be expressed as [21]:

$$u_{s\alpha,\beta} = \frac{2}{3} u_{DC}(S_a + aS_b + a^2 S_c) \tag{5}$$

$$a = e^{j\frac{2\pi}{3}} \tag{6}$$

where u_{DC} is the dc-link voltage.

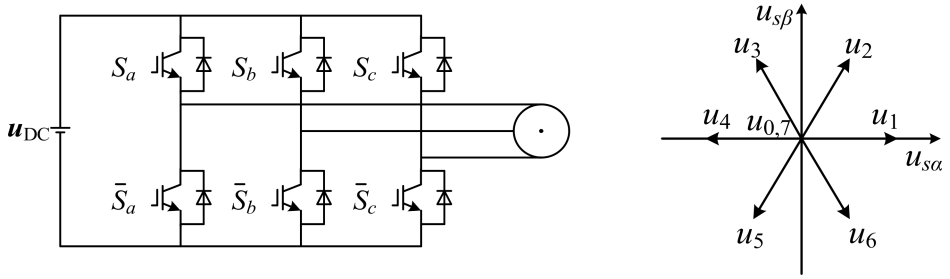

Figure 1. The topology of 2-L VSI and the applied voltage vectors. (**a**) 2-L VSI. (**b**) applied voltage vectors.

3. Multistep PCC Algorithm

In the PCC algorithm, the tracking error between the predicted stator current and its reference value is considered as the predominant control target. The additional constraints, i.e., the limitations of switching frequency and current magnitude, are included in the cost function of the PCC algorithm. According to the IM model, the stator current is rewritten as:

$$i_{s\alpha,\beta} = -\frac{1}{R_\sigma}((L_\sigma \frac{\mathrm{d}i_{s\alpha,\beta}}{\mathrm{dt}} - k_r(\frac{1}{\tau_r} - j\omega) \cdot \psi_{r\alpha,\beta}) - u_{s\alpha,\beta}) \tag{7}$$

where the rotor coupling factor $k_r = L_m/L_r$, rotor time constant $\tau_r = L_r/R_r$, effective resistance of both windings $R_\sigma = R_s + {k_r}^2 \cdot R_r$, leakage coefficient $\sigma = 1 - ({L_m}^2/L_sL_r)$ and

transient stator inductance $L_\sigma = \sigma \cdot L_s$. The predicted value of stator current can be obtained by forward Euler discretization.

$$\frac{\mathrm{d}i_{s\alpha,\beta}(k)}{\mathrm{d}t} = \frac{\hat{i}_{s\alpha,\beta}(k+1) - i_{s\alpha,\beta}(k)}{T_s} \tag{8}$$

where T_s is the sampling period. Therefore, the predicted stator current is described in Equation (9).

$$\hat{i}_{s\alpha,\beta}(k+1) = (1 - \frac{T_s}{\tau_\sigma})i_{s\alpha,\beta}(k) + \frac{T_s}{\tau_\sigma R_\sigma} \cdot [k_r \cdot (\frac{1}{\tau_r} - j\omega(k)) \cdot \psi_{r\alpha,\beta}(k) + u_{s\alpha,\beta}(k)] \tag{9}$$

where $\tau_\sigma = \sigma L_s / R_\sigma$. To compensate for the time delay in the PCC algorithm, the predicted stator current at $k+2$ interval is expressed as [22]:

$$\begin{aligned} \hat{i}_{s\alpha,\beta}(k+2) \quad &= (1 - \tfrac{T_s}{\tau_\sigma})\hat{i}_{s\alpha,\beta}(k+1) + \tfrac{T_s}{\tau_\sigma R_\sigma} \cdot [k_r \cdot (\tfrac{1}{\tau_r} - j\omega(k)) \cdot \hat{\psi}_{r\alpha,\beta}(k+1) \\ &+ u_{s\alpha,\beta}(k+1)] \end{aligned} \tag{10}$$

As the number of prediction horizons is N, the cost function of the multistep PCC algorithm is expressed as:

$$g = \sum_{h=2}^{N+1} \{(i^*_{s\alpha} - i_{s\alpha}(k+h))^2 + (i^*_{s\beta} - i_{s\beta}(k+h))^2 + \lambda^2_{sw} \cdot n^2_{sw} + \mathrm{Im}(k+h)\} \tag{11}$$

in which the stator current error, the constraints of switching frequency and current magnitude are included. n_{sw} is the number of switching events in a sampling period. The reference value of the stator current in the stationary $\alpha\beta$ frame can be expressed as

$$\begin{bmatrix} i^*_{s\alpha} \\ i^*_{s\beta} \end{bmatrix} = \begin{bmatrix} \cos\theta & -\sin\theta \\ \sin\theta & \cos\theta \end{bmatrix} \begin{bmatrix} \frac{|\psi^*_r|}{L_m} \\ \frac{2L_r T^*}{3L_m |\psi^*_r|} \end{bmatrix} \tag{12}$$

where the flux angle $\theta = \arctan(\psi_{r\alpha}/\psi_{r\beta})$ and $|\psi_r{}^*|$ represents the reference of rotor flux. The current magnitude limitation is described in Equation (13). As shown in Equation (13), the current limitation term $\mathrm{Im}(k+h)$ is infinity when the stator current magnitude $|i_s(k+h)|$ is larger than the limitation $|i_{smax}|$. The close-loop block diagram of the multistep PCC algorithm is shown in Figure 2. The reference is denoted by the superscript *, T represents the electromagnetic torque.

$$\mathrm{Im}(k+h) = \begin{cases} 0, & |i_s(k+h)| \le |i_{\mathrm{smax}}| \\ \infty, & |i_s(k+h)| > |i_{\mathrm{smax}}| \end{cases} \tag{13}$$

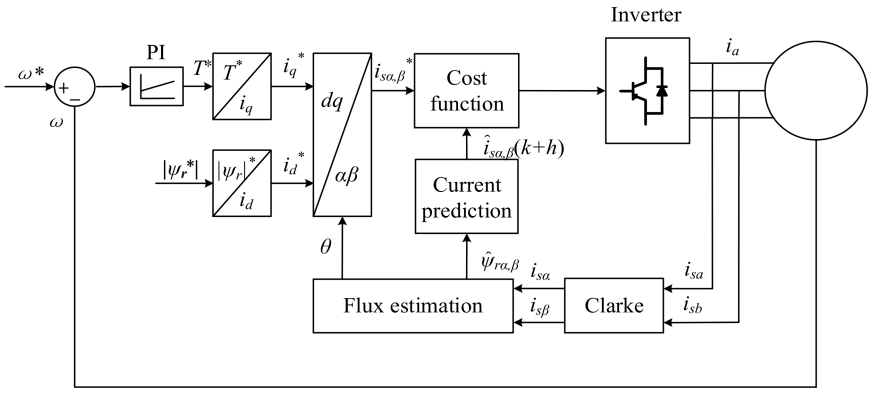

Figure 2. Close-loop block diagram of the multistep PCC algorithm.

In regards to the predominant control target of the PCC optimization problem minimizing the error between the predicted stator current and its reference value, the geometric description of the PCC optimization problem is shown in Figure 3. As can be seen, $i_{s\alpha,\beta}(k+h)$ is the predicted stator current at $h-1$ interval, $i_{s\alpha,\beta}{}^{*}$ is the reference value and $d(k+h)$ denotes the tracking error between the predicted and reference value. Therefore, the tracking error term of the stator current can be regarded as the quadratic Euclidean norm of $d(k+h)$, which is formulated as:

$$||d(k+h)||_2^2 = (i_{s\alpha}^* - i_{s\alpha}(k+h))^2 + (i_{s\beta}^* - i_{s\beta}(k+h))^2 \tag{14}$$

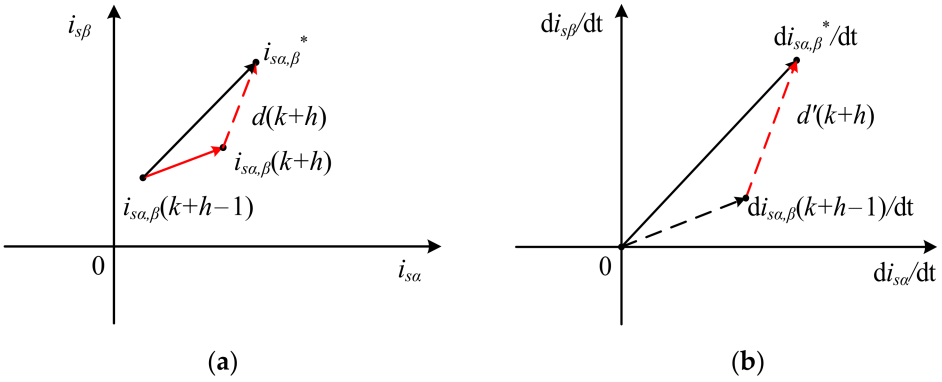

Figure 3. Geometric description of the PCC optimization problem. (**a**) Stator current. (**b**) Projection on stator current derivative.

We can obtain Figure 3b as Figure 3a is projected on the current derivative plane. As shown in Figure 3b, the distance between the predicted and reference derivative value is $d'(k+h)$. The quadratic Euclidean norm of $d'(k+h)$ is expressed as:

$$||d\prime(k+h)||_2^2 = \left(\frac{\mathrm{d}i_{s\alpha}^*}{\mathrm{dt}} - \frac{\mathrm{d}i_{s\alpha}(k+h)}{\mathrm{dt}}\right)^2 + \left(\frac{\mathrm{d}i_{s\beta}^*}{\mathrm{dt}} - \frac{\mathrm{d}i_{s\beta}(k+h)}{\mathrm{dt}}\right)^2 \tag{15}$$

Based on the above, the multistep PCC optimization problem is considered as a quadratic programming (QP) problem. The cost function of multistep PCC is rearranged as:

$$g\prime = \sum_{h=1}^{N}\left\{\left(\frac{\mathrm{d}i_{s\alpha}^*}{\mathrm{dt}} - \frac{\mathrm{d}i_{s\alpha}(k+h)}{\mathrm{dt}}\right)^2 + \left(\frac{\mathrm{d}i_{s\beta}^*}{\mathrm{dt}} - \frac{\mathrm{d}i_{s\beta}(k+h)}{\mathrm{dt}}\right)^2 + \lambda_{sw}^2 \cdot n_{sw}^2 + \mathrm{Im}(k+h)\right\} \tag{16}$$

4. Fast Quadratic Programming Solution

To tackle the issue that the number of searched control inputs grows exponentially with the increased number of prediction horizons, a fast quadratic solution is proposed in this paper for algorithm complexity reduction instead of the exhaustive search.

The preselection principle of the fast quadratic programming solver is shown in Figure 4. First, the current derivatives $\mathrm{d}i_s(k+h-1)/\mathrm{dt}_j$ using the different voltage vectors (j = 0,1, . . . ,6) as well as the reference derivative $\mathrm{d}i_s{}^{*}/\mathrm{dt}$ are calculated. The error of the angle ($|\theta_j - \theta^*|$) between the applied current derivative and the reference derivative is evaluated. Two derivative vectors that minimize the error $|\theta_j - \theta^*|$ are selected as the preselection vectors. In each prediction horizon, the cost function (16) is optimized for the two preselection vectors.

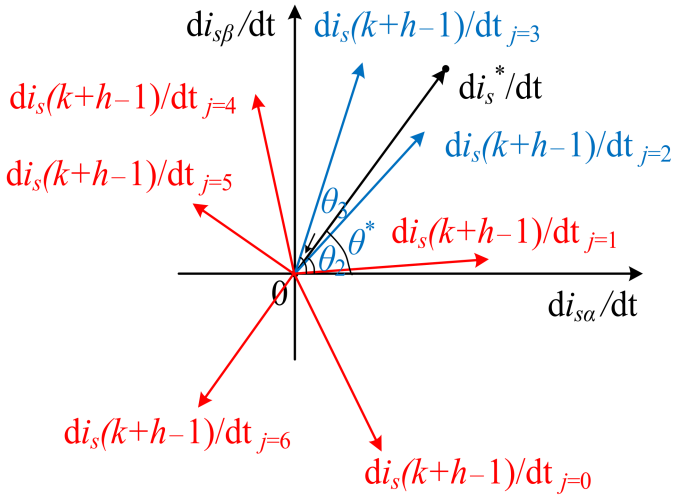

Figure 4. Preselection principle of the fast quadratic programming solver.

As shown in Figure 5, the preselection-principle-based search method for the multistep PCC algorithm is proposed. As can be seen, the red nodes are the preselection vectors to be optimized. The black nodes are the unvisited vectors that will not participate in the optimization procedure. Assuming that the number of prediction horizon $h - 1 = N$, the number of searched nodes is $\eta_1 = 7^N$. The number of preselection vectors for optimization is $\eta_2 = 2^N$ when the proposed fast quadratic programming solver is applied. The comparisons of optimization number between exhaustive search and fast QP solution are summarized in Table 1.

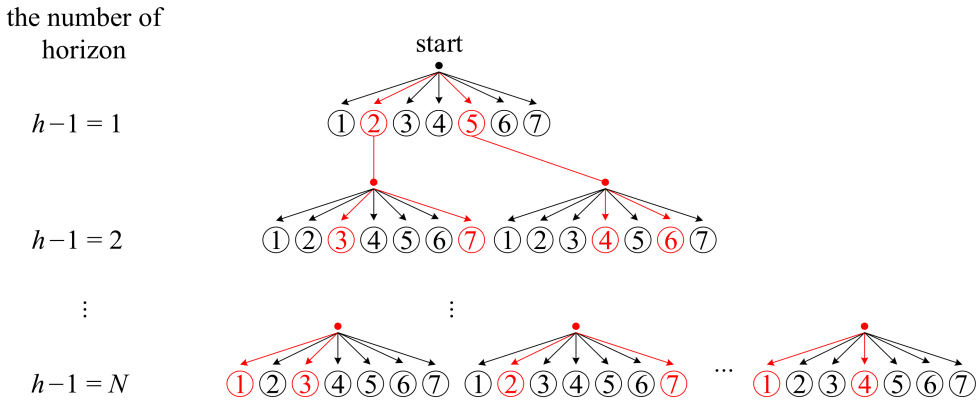

Figure 5. Preselection-principle-based search method in multistep PCC algorithm.

Table 1. Comparisons of optimization number between exhaustive search and fast QP solution.

Number of Prediction Horizons	Exhaustive Search η_1	Fast QP Solution η_2	η_1/η_2/%
1	7	2	28.57
2	49	4	8.16
3	343	8	2.33
4	2401	16	0.67
5	16,807	32	0.19

5. Experimental Verification

The proposed fast QP solution for the multistep PCC algorithm is experimentally implemented on the 2.2 kW IM drive testbench, as shown in Figure 6. The components of the testbench are listed in Table 2. The parameters of IM are illustrated in Table 3. A 1.4 GHz self-made Linux-based real-time control system is applied to conduct the proposed

algorithm. The applied sampling period T_s is 62.5 µs. The applied control system has competitive computational capability with the commercial processors, e.g., DSP, FPGA and Ultrazphm.

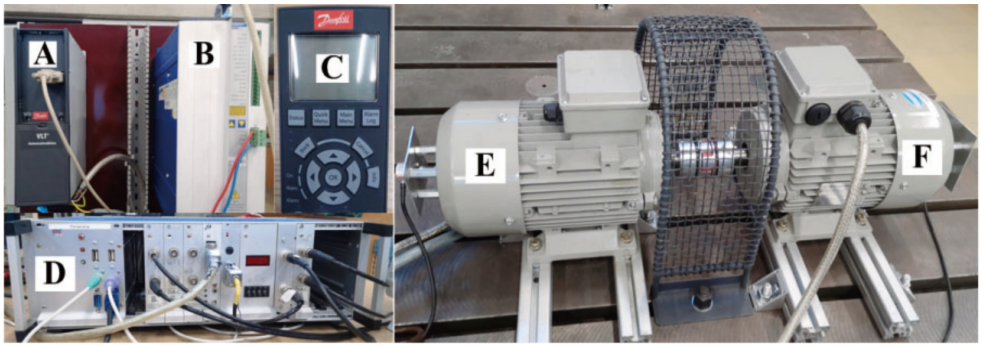

Figure 6. Experimental testbench description. (A) Danfoss inverter. (B) Servostar inverter. (C) Control panel. (D) Real-time control system. (E) Main machine. (F) Load Machine.

Table 2. The components of the experimental testbench.

Number	Description
A	Danfoss inverter (3.0 kW)
B	Servostar inverter (14 kVA)
C	Control panel
D	1.4 GHz Linux-based real-time control system
E	Main machine (2.2 kW IM)
F	Load machine (2.2 kW IM)

Table 3. Induction machine parameters.

Parameter	Value
DC-link voltage u_{DC}/V	582
Nominal rotor speed ω_{nom}/rpm	2772
Nominal torque T_{nom}/Nm	7.5
Nominal flux $\|\|\psi_{nom}\|\|$/Wb	0.71
Nominal rated power P_{nom}/kW	2.2
Stator, rotor resistance R_s, R_r/Ω	2.68, 2.13
Stator, rotor inductance L_s, L_r/H	0.283, 0.283
Magnetizing inductance L_m/H	0.275
Number of pole pairs p	1
PI parameters k_p, k_i	0.23, 5.38

Figure 7 shows the comparisons between the steady-state performance of multistep PCC with a fast QP solution and the conventional PCC method at 200 rpm with a 2 Nm load torque. The switching frequency is 800 Hz. Figure 7a shows the measured waveforms of conventional PCC. It can be observed that conventional PCC suffers from the high torque and current ripples, which are 2.0 Nm and 0.56 A, respectively. The measured waveforms of the proposed multistep PCC with a fast QP solution are shown in Figure 8b. The torque and current ripples are 1.6 Nm and 0.33 A, respectively. Experimental results confirm that the proposed multistep PCC with a fast QP solution achieves a smaller torque and current error when compared with conventional PCC at a similar switching frequency.

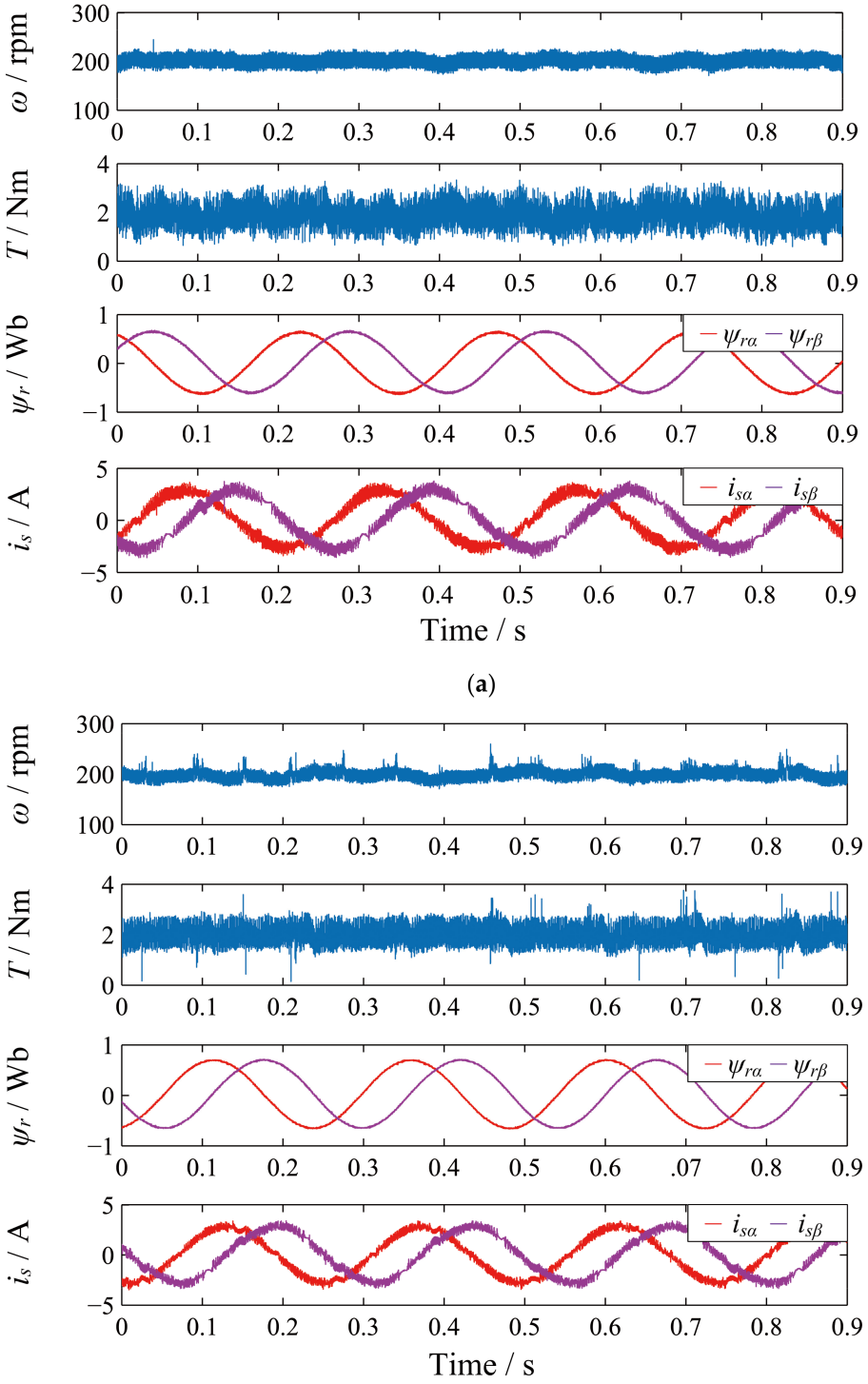

Figure 7. Steady-state performance of two predictive current control schemes (ω = 200 rpm, T = 2 Nm). (**a**) Conventional PCC. (**b**) Proposed multistep PCC wth a fast QP solution.

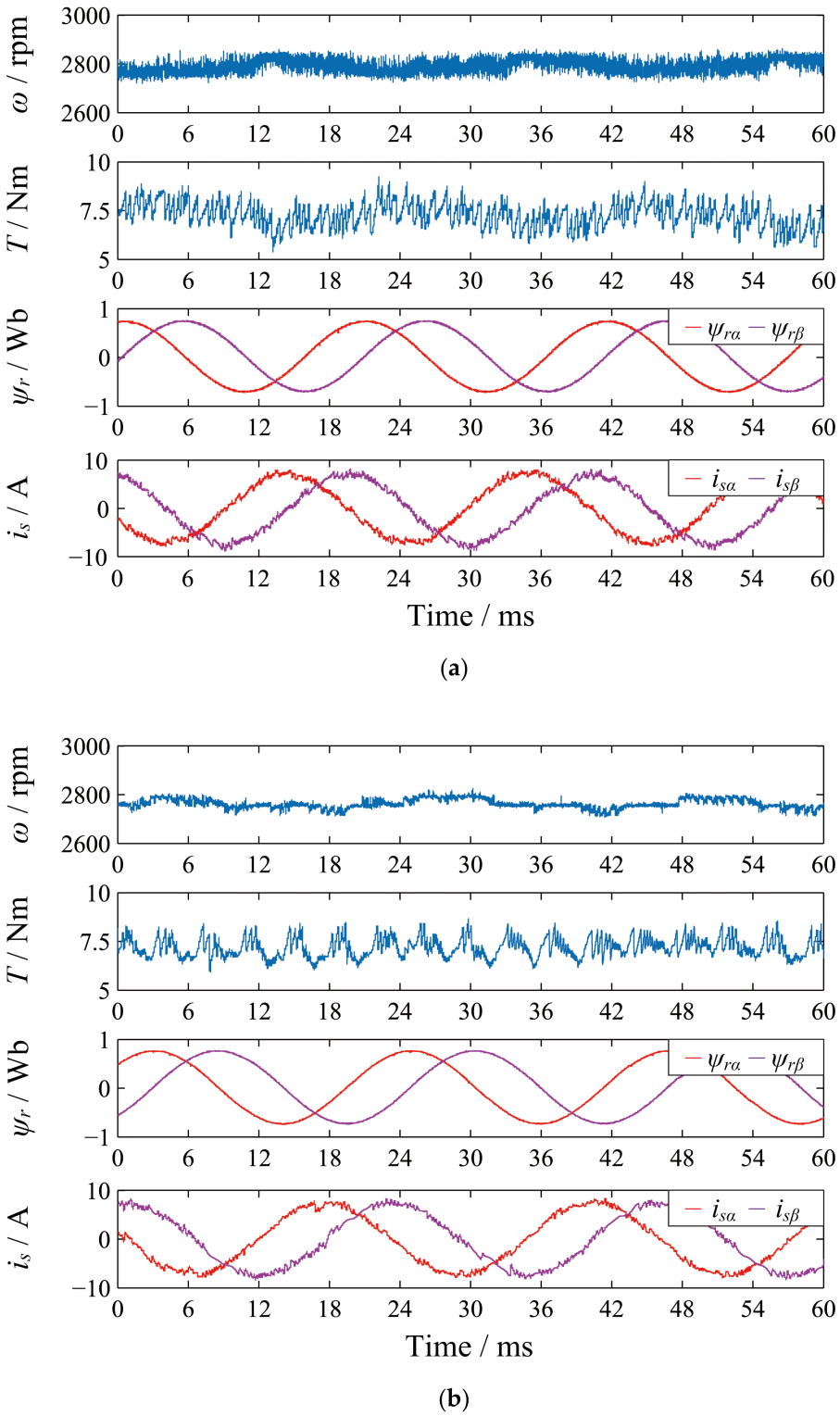

Figure 8. Steady-state performance of two predictive current control schemes (ω = 2772 rpm, T = 7.5 Nm). (**a**) Conventional PCC. (**b**) Proposed multistep PCC with a fast QP solution.

Figure 8 shows the steady state performance of the two PCC methods at the nominal rotor speed and load torque (ω = 2772 rpm, T = 7.5 Nm). Due to the optimal solution in a longer prediction horizon, the proposed algorithm obtains a 29 % and 24 % reduction on torque and current tracking errors. As shown in Figure 8b, the current error of the proposed algorithm is 0.62 A. Both the switching frequencies of the two PCC algorithms in

the nominal steady-state scenario are 1.8 kHz. It is validated that the proposed algorithm has better current quality in both the steady-state scenarios. The comparisons of performae metric between the conventonal PCC and the proposed algorithm are summarized in Table 4.

Table 4. Comparisons of the performance metric between the conventional PCC and the propo sed algorithm.

Test Scenarios	Performance Metric	Conventional PCC	Proposed Algorithm
1	Torque ripple	2.0 Nm	1.6 Nm
	Current ripple	0.56 A	0.33 A
2	Torque ripple	2.5 Nm	1.8 Nm
	Current ripple	0.81 A	0.62 A

Figure 9 shows the load disturbance performance of the proposed multistep PCC algorithm with a fast QP solution. The IM operates at a 50% nominal rotor speed (1386 rpm). At t = 170 ms, a 4 Nm load torque is applied by the control panel. As can be seen in Figure 9, the proposed algorithm has a fast dynamic response in which the load torque rises from 0 Nm to 4 Nm in 28 ms. Meanwhile, the rotor speed decreases from 1386 rpm to 1280 rpm, and then recovers to the original value in 190 ms. After the load disturbance transience, the proposed algorithm achieves an excellent steady-state performance in which the torque and current errors are 1.8 Nm and 0.44 Nm, respectively.

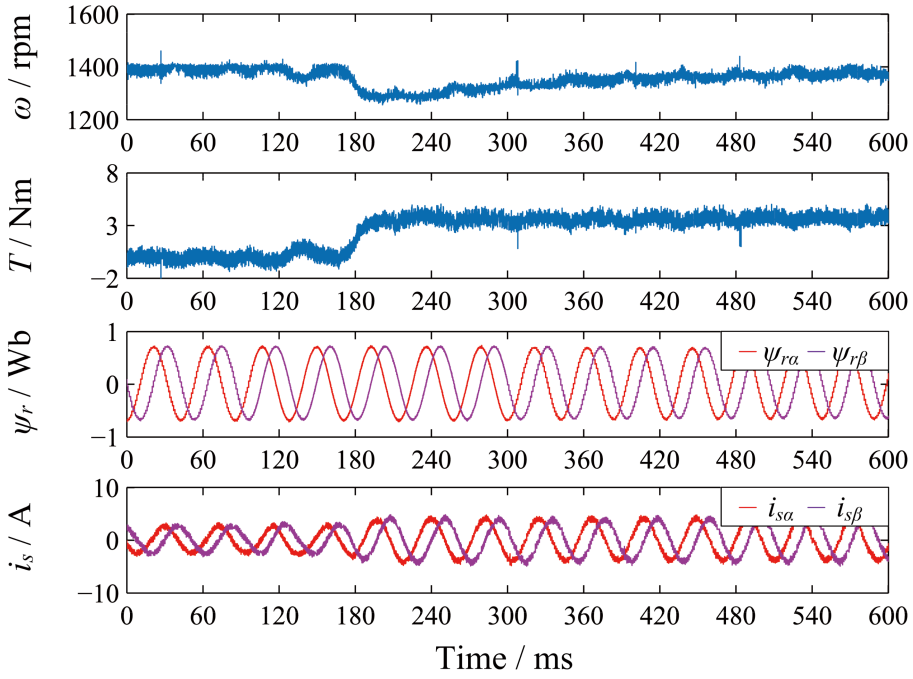

Figure 9. Load disturbance performance of multistep PCC with a fast QP solution (ω = 1386 rpm, T = 4 Nm).

In Figure 10, the load step performance of the proposed algorithm is presented. The speed control mode is employed in which an 800 rpm rotor speed is given by the control panel. A 2 Nm load torque is applied by the algorithm, which changes to 4 Nm at t = 187 ms. It can be observed in Figure 10 that the rotor speed increases from 800 rpm to 980 rpm (a 22.5% increase). The rotor speed returns to the original value at t = 540 ms while the recovery time is 353 ms. More specifically, the load step is completed in 300 µs while the torque error is 1.3 Nm. The current error of the proposed algorithm in this test scenario is 0.40 A. The transient-state performance verifies that the proposed multistep PCC with a fast QP solution achieves a fast dynamic response and a small steady-state tracking error.

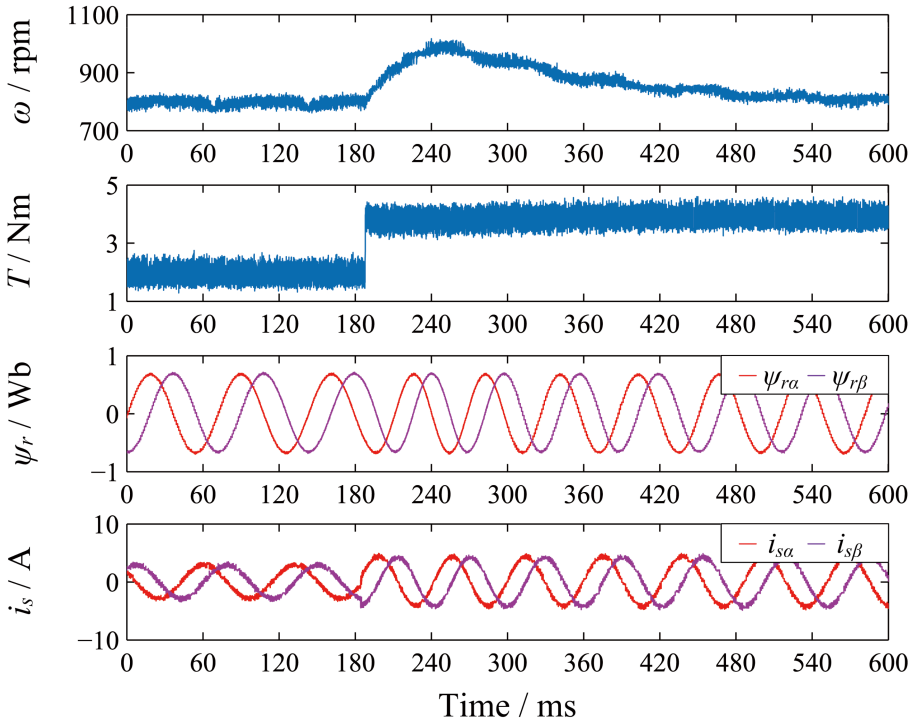

Figure 10. Load step performance of multistep PCC with a fast QP solution (ω = 800 rpm, T changes from 2 to 4 Nm).

The comparisons between the number of optimized nodes and algorithm time for the proposed algorithm and conventional PCC are illustrated in Table 5. As shown in Table 5, the number of optimized nodes in the conventional PCC is 7. The algorithm time of the conventional PCC is 19 µs. On the contrary, the proposed algorithm with a prediction horizon of 5 has 32 optimized nodes, which requires a 27 µs algorithm time. Compared with the exhaustive search in Table 1, the number of nodes in the proposed algorithm is significantly reduced by 99.81 %. The proposed algorithm can be implemented at the same sampling period (T_s = 62.5 µs) as that of conventional PCC.

Table 5. Comparisons between the number of optimized nodes and algorithm time of the two methods.

Algorithm	Number of Optimized Nodes	Algorithm Time
Conventional PCC	7	19 µs
Proposed multistep PCC with a fast QP solution	32	27 µs

6. Conclusions

This paper proposes a fast quadratic programming (QP) solution for the multistep predictive current control (PCC) algorithm. Compared with the conventional PCC method, the proposed algorithm achieves a better steady-state performance and retains a fast dynamic response. Moreover, the number of optimized nodes as well as the algorithm time is significantly reduced. In the proposed algorithm, the PCC optimization problem is regarded as a QP problem. The cost function is formulated as the quadratic Euclidean norm of the distance between the predicted and reference value. To reduce the algorithm time, two vectors are preselected by minimizing the error of angle. The optimization procedure is applied with the preselection vectors in each prediction horizon. Experimental results verified that the proposed algorithm has the merits of better steady-state performance, fast dynamic response and low algorithm complexity. Moreover, the proposed fast QP solution for the multistep PCC algorithm can be extended to the multilevel converter applications in which the number of control inputs is higher.

Author Contributions: Conceptualization, H.X. and F.W.; methodology, H.X., J.D. and Y.H.; software, H.X.; validation, H.X., J.D. and Y.H.; formal analysis, D.K.; data curation, H.X.; writing—original draft preparation, H.X.; writing—review and editing, D.K. and C.H.; supervision, J.R. and R.K.; project administration, R.K.; funding acquisition, F.W. All authors have read and agreed to the published version of the manuscript.

Funding: This research was funded in part by the National Natural Science Funds of China, grant number 51877207, in part by the Quanzhou Science and Technology Project, grant number 2020C002R and 2020C073 and in part by the ANID through Chilean projects, grant number FB0008, ACT192013 and 1210208.

Institutional Review Board Statement: Not applicable.

Informed Consent Statement: Not applicable.

Data Availability Statement: Not applicable.

Acknowledgments: The authors acknowledge the support of ANID through projects FB0008, ACT 192013 and 1210208.

Conflicts of Interest: The authors declare no conflict of interest. The funders had no role in the design of the study; in the collection, analyses, or interpretation of data; in the writing of the manuscript, or in the decision to publish the results.

References

1. Mayne, D.Q. Model Predictive Control: Recent Developments and Future Promise. *Automatica* **2014**, *50*, 2967–2986. [CrossRef]
2. Rao, C.V.; Rawlings, J.B.; Mayne, D.Q. Constrained state estimation for nonlinear discrete-time systems: Stability and moving horizon approximations. *IEEE Trans. Autom. Control* **2003**, *48*, 246–258. [CrossRef]
3. Wang, Y.; Boyd, S. Fast Model Predictive Control Using Online Optimization. *IEEE Trans. Control. Syst. Technol.* **2010**, *18*, 267–278. [CrossRef]
4. Xu, Y.; Tang, W.; Chen, B.; Qiu, L.; Yang, R. A Model Predictive Control with Preview-Follower Theory Algorithm for Trajectory Tracking Control in Autonomous Vehicles. *Symmetry* **2021**, *13*, 381. [CrossRef]
5. Ji, H.; Wei, Y.; Fan, L.; Liu, S.; Wang, Y.; Wang, L. Disturbance-Improved Model-Free Adaptive Prediction Control for Discrete-Time Nonlinear Systems with Time Delay. *Symmetry* **2021**, *13*, 2128. [CrossRef]
6. Xi, Y.; Li, D.; Lin, S. Model predictive control—Status and Challenges. *Acta Autom. Sin.* **2013**, *39*, 222–236. [CrossRef]
7. Bemporad, A.; Borrelli, F.; Morari, M. Model predictive control based on linear programming—The explicit solution. *IEEE Trans. Autom. Control* **2002**, *47*, 1974–1985. [CrossRef]
8. Vazquez, S.; Rodriguez, J.; Rivera, M.; Franquelo, L.G.; Norambuena, M. Model predictive control for power converters and drives: Advances and Trends. *IEEE Trans. Ind. Electron.* **2017**, *64*, 935–947. [CrossRef]
9. Zhang, Z.; Babayomi, O.; Dragicevic, T.; Heydari, R.; Garcia, C.; Rodriguez, J.; Kennel, R. Advances and opportunities in the model predictive control of microgrids: Part I—primary layer. *Int. J. Electr. Power Energy Syst.* **2022**, *134*, 107411. [CrossRef]
10. Ahmed, A.A.; Koh, B.K.; Lee, Y.I. A Comparison of Finite Control Set and Continuous Control Set Model Predictive Control Schemes for Speed Control of Induction Motors. *IEEE Trans. Ind. Inform.* **2018**, *14*, 1334–1346. [CrossRef]
11. Zhou, J.; Hassan, M.A.; Zhang, J.; Hou, M.; Wu, S.; Xing, G.; Chi, S. Stabilization of Constant Power Loads in DC Microgrid Systems Using an Adaptive Continuous Control Set Model Predictive Control. *Symmetry* **2021**, *13*, 1112. [CrossRef]
12. Karamanakos, P.; Geyer, T. Guidelines for the Design of Finite Control Set Model Predictive Controllers. *IEEE Trans. Power Electron.* **2020**, *35*, 7434–7450. [CrossRef]
13. Karamanakos, P.; Liegmann, E.; Geyer, T.; Kennel, R. Model Predictive Control of Power Electronic Systems: Methods, Results, and Challenges. *IEEE Open J. Ind. Appl.* **2020**, *1*, 95–114. [CrossRef]
14. Wang, F.; Li, S.; Mei, X.; Xie, W.; Rodriguez, J.; Kennel, R. Model-based Predictive Direct Control Strategies for Electrical Drives: An Experimental Evaluation of PTC and PCC Methods. *IEEE Trans. Ind. Inform.* **2015**, *11*, 671–681. [CrossRef]
15. Zhang, Y.; Jiang, T. Robust Predictive Rotor Current Control of a Doubly Fed Induction Generator Under an Unbalanced and Distorted Grid. *IEEE Trans. Energy Convers.* **2022**, *37*, 433–442. [CrossRef]
16. Geyer, T.; Papafotiou, G.; Morari, M. Model Predictive Direct Torque Control—Part I: Concept, Algorithm, and Analysis. *IEEE Trans. Ind. Electron.* **2009**, *56*, 1894–1905. [CrossRef]
17. Geyer, T.; Quevedo, D.E. Performance of Multistep Finite Control Set Model Predictive Control for Power Electronics. *IEEE Trans. Power Electron.* **2015**, *30*, 1633–1644. [CrossRef]
18. Zhang, Z.; Hackl, C.M.; Kennel, R. Computationally Efficient DMPC for Three-Level NPC Back-to-Back Converters in Wind Turbine Systems with PMSG. *IEEE Trans. Power Electron.* **2017**, *32*, 8018–8034. [CrossRef]
19. Baidya, R.; Aguilera, R.P.; Acuña, P.; Vazquez, S.; Mouton, H.D.T. Multistep Model Predictive Control for Cascaded H-Bridge Inverters: Formulation and Analysis. *IEEE Trans. Power Electron.* **2018**, *33*, 876–886. [CrossRef]

20. Dorfling, T.; Mouton, H.d.T.; Geyer, T.; Karamanakos, P. Long-horizon Finite-Control-Set Model Predictive Control with Nonrecursive Sphere Decoding on an FPGA. *IEEE Trans. Power Electron.* **2020**, *35*, 7520–7531. [CrossRef]
21. Zhou, Z.; Xia, C.; Yan, Y.; Wang, Z.; Shi, T. Torque Ripple Minimization of Predictive Torque Control for PMSM With Extended Control Set. *IEEE Trans. Ind. Electron.* **2017**, *64*, 6930–6939. [CrossRef]
22. Gao, J.; Gong, C.; Li, W.; Liu, J. Novel Compensation Strategy for Calculation Delay of Finite Control Set Model Predictive Current Control in PMSM. *IEEE Trans. Ind. Electron.* **2020**, *67*, 5816–5819. [CrossRef]